Volume 7 | Number 4 | 28 January 2015 | Pages 1239–1512

Nanoscale

www.rsc.org/nanoscale

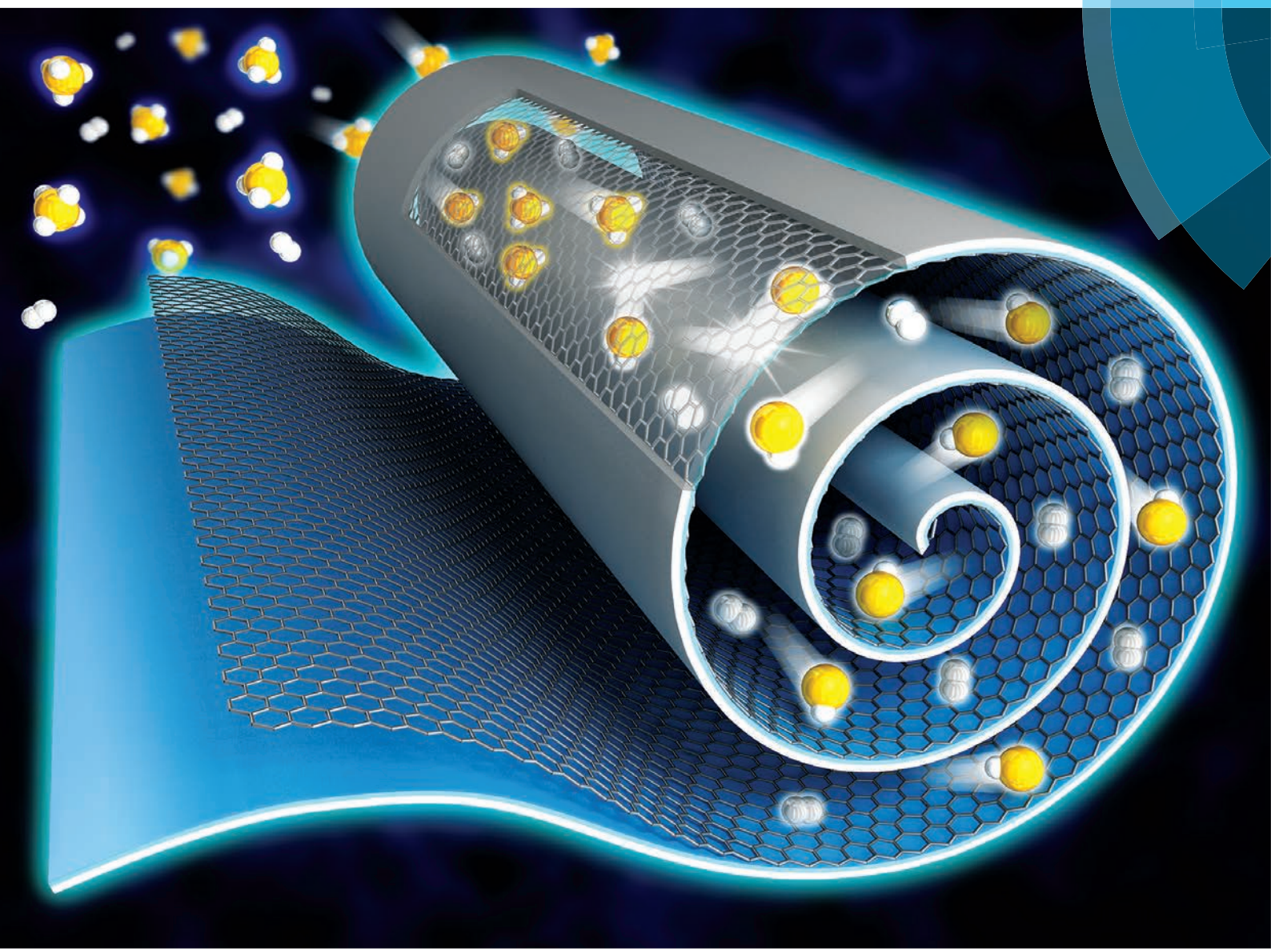

ISSN 2040-3364

ROYAL SOCIETY OF CHEMISTRY

PAPER
Kilwon Cho *et al.*
Graphene growth under *Knudsen* molecular flow on a confined catalytic metal coil

NCNST

Published on 29 September 2014. Downloaded by Pohang University of Science and Technology on 18/07/2015 09:21:24.

Nanoscale

PAPER

View Article Online
View Journal | View Issue

Cite this: *Nanoscale*, 2015, **7**, 1314

Graphene growth under *Knudsen* molecular flow on a confined catalytic metal coil†

Hyojin Bong,‡ Sae Byeok Jo,‡ Boseok Kang, Seong Kyu Lee, Hyun Ho Kim, Seung Goo Lee and Kilwon Cho*

Received 22nd July 2014,
Accepted 28th September 2014

DOI: 10.1039/c4nr04153d

www.rsc.org/nanoscale

We have established a simple method for drastically improving the productivity of chemical vapor deposition in large-area graphene synthesis using a roll-stacked Ni coil as a catalyst. Our systematic investigation of the effects of a confined catalytic geometry has shown that the gas flow through interfacial gaps within the stack follows non-continuum fluid dynamics when the size of the gap decreases sufficiently, which enhances the dissolution of the carbon sources into the catalyst during synthesis. Quantitative criteria for graphene growth in the confined geometry are established through the introduction of the *Knudsen* number, *Kn*, which is the ratio of the mean-free-path of the gas molecules to the size of the gap. The criteria provided in this article for the synthesis of graphene in the confined geometry are expected to provide the foundations for the efficient mass production of large-area graphene. We also show that the evolution of the catalytic Ni surface in a stacked system results in larger grains in the (111) plane, and consequently in reproducible, uniform, and high-quality multi-layered graphene.

1. Introduction

Graphene consists of two-dimensional carbon atoms with sp^2 bonds; it has excellent mechanical,[1] thermal,[2] optical,[3] and electrical properties.[4–7] There are many methods for the synthesis of graphene including the mechanical exfoliation of graphite,[8] epitaxial growth on SiC,[9–12] and chemical vapor deposition (CVD).[13–15] The CVD of hydrocarbon gases onto a sheet of a transition-metal catalyst produces graphene that possesses high quality, large sheet size, and transferability to arbitrary substrates. However, the dimensions of the resulting graphene sheet are constrained by the surface area of the metal catalyst, which sets limits on large-area graphene synthesis.[13,15–18]

To obtain large-area graphene by CVD, the synthetic process must be organized, including the synthesis of graphene and consecutive transfer to arbitrary substrates. In a previous study, a 30 inch Cu foil was used for large-area graphene synthesis, and the acquired graphene was easily transferred to various substrates using a simple wet-transfer method with a polymer supporting layer.[16] However, this process requires the foils to be separated from each catalytic surface, because the synthesis temperature (900–1000 °C) is close to the melting point of Cu (1085 °C) so that Cu surfaces in close proximity can easily weld together. Therefore, the size of a CVD chamber depends on the required graphene sheet size; the size of the chamber must be increased to achieve larger graphene. A continuous synthetic method, such as the roll-to-roll (R2R) based CVD process, has been demonstrated to scale up the graphene synthesis.[19] The R2R process does not require simultaneous heating of the entire catalyst surface, so the simple unrolling of a catalytic metal coil enables the synthesis of graphene sheets up to 100 m in length,[19] and also continuous transfer to flexible substrates.[16] However, in continuous synthetic methods, it is easily overlooked that the required deposition time and the thermal energy consumption increase in proportion to the area of the graphene, which is critical to the efficient synthesis of large-area graphene.

To resolve these issues while preserving the promising characteristics of both the conventional one-pot synthesis process and the continuous R2R process,[20,21] an approach that enables the incorporation of various catalyst geometries such as a catalyst stacking with appropriate spacing for efficient spatial usage of the chamber needs to be developed. Moreover, for the stacked catalyst geometry, more sophisticated considerations of the gas flow behavior are required than for a conventional open non-stacked system. In this confined catalytic system, gas flows through narrow gaps between the catalytic surfaces, so the gas flow behavior and surface reactions on the catalyst surfaces are different from those in the open non-stacked system. Previous research has studied the mass transport of carbon sources in the CVD of graphene using the

Department of Chemical Engineering, Pohang University of Science and Technology, Pohang 790-784, Korea. E-mail: kwcho@postech.ac.kr

†Electronic supplementary information (ESI) available. See DOI: 10.1039/c4nr04153d

‡H. Bong and S. B. Jo contributed equally to this work.

This journal is © The Royal Society of Chemistry 2015

Published on 29 September 2014. Downloaded by Pohang University of Science and Technology on 18/07/2015 09:21:24.

boundary layer concepts of fluid mechanics.[22–25] However, these concepts could not be applied to this confined gap system, because the gas flow does not follow the conventional continuum-flow regime including the boundary layer concepts when the gap size is on the micron scale. Under these conditions, the flow changes to a non-continuum regime since the viscous force exerted on each wall becomes dominant as the dimension of the fluidic system decreases. In the non-continuum regime, each individual gas molecule collides more frequently with the walls of the stack than with other gas molecules. Thus, the gas flow in the confined geometry should be described with a quantity that takes into account the dimensions of the system. Therefore, the *Knudsen* number, *Kn*, which is the ratio of the molecular mean free path to the characteristic dimension of the system, was recommended as a new parameter that takes into account the interfacial gap size. Taking the above considerations into account, we designed an efficient synthetic method in which a roll-stacked catalytic metal coil is incorporated into the one-pot CVD process to simultaneously maximize the catalytic area and minimize unnecessary time and energy consumption. Moreover, we also thoroughly investigated the graphene growth mechanism for the confined catalytic surface with this unconventional geometry. We used a thermally evaporated Ni (melting point 1453 °C) substrate on a flexible stainless steel (SUS) and Si wafer to prevent the catalyst sheets from sticking together during the process. Graphene grown on the roll-stacked Ni catalytic coil has reproducible, uniform properties. We also constructed a system consisting of stacked substrates as a simplified model of the roll-stacked Ni coil, and systematically studied the mass transport mechanism in the stacked system. Quantitative criteria for graphene growth in the confined geometry under a specific flow regime were determined. Moreover, the metal catalyst surface quality was analyzed to determine how the gap size in the stacked system affects the properties of the synthesized graphene.

2. Experimental section

2.1 Graphene growth

To fabricate a roll-stacked Ni/SUS coil, a 500 nm SiO_2 layer was deposited by PECVD and then a 400 nm Ni film was deposited by thermal evaporation onto the stainless steel (SUS) substrate. In the multi-layered or two-layered stacked systems, 400 nm Ni layers were deposited onto each SiO_2/Si substrate (300 nm SiO_2) using a thermal evaporator. Ni sources (purity > 99.995%) were purchased from Alfa Aesar®. The Ni-evaporated substrates were loaded into an inner quartz tube (diameter 1") inside a chemical vapor depositor under vacuum. When the temperature of the furnace reached 900 °C, the substrates were moved into it rapidly and a flow of mixed gases was introduced through a tube. The mixed gases consisted of methane, hydrogen and argon; the CH_4 gas flow rate was adjusted from 2 to 50 sccm (H_2 : Ar = 100 : 500 sccm), which corresponds to a CH_4 concentration in the range 0.33 vol% to 7.69 vol%. After 10 minutes of growth, the substrates bearing graphene were removed from the furnace quickly and cooled to room temperature in hydrogen gas.

2.2 Graphene transfer

To transfer a graphene film to an arbitrary substrate such as a SiO_2/Si wafer or glass, polymethyl methacrylate (PMMA) was coated onto the graphene grown on the Ni surface as a supporting layer. The SiO_2 layer was etched out with dilute HF and the Ni film was etched out with $FeCl_3$. The graphene/PMMA film was washed in deionized water to remove the etchant, and then transferred to the substrate. Finally, we used chloroform to remove the PMMA.

2.3 Gap fabrication

To adjust the gap sizes, we fabricated trench structures with the SiO_2/Si wafers. First, the SiO_2 layer was removed using HF, and 2 mm ridges were left on both sides of the wafers. Then, the Si layer was etched using a mixed solution of HF and HNO_3 (1 : 3 *vol/vol*). By varying the etching time, we obtained gap sizes of 520 nm and 30 μm. The gap sizes of 600 μm and 1.2 mm were obtained by placing one and two 600 μm thick wafer pieces between substrates.

2.4 Characterization

The morphologies of the graphene films were characterized with an optical microscope (Axioplan, Zeiss). Raman spectroscopy was conducted at a wavelength of 532 nm (WITec, Micro Raman). The film transmittances were determined using UV-visible irradiation in transmittance mode. The sheet resistances were determined with a four-point probe tester. The Ni morphologies were obtained using an atomic force microscope (Digital Instruments Multimode Nanoscope III) in tapping mode. Normal mode X-ray diffraction (XRD) measurements were performed (wavelength 0.108 nm) at the Pohang Accelerator Laboratory (PAL) in Korea. Electron Backscatter Diffraction (EBSD) was installed on a focused ion beam (FEI Helios, Pegasus). EBSD analyses were performed with a step size of 5 nm, and the data were post-processed using the TSL® OIM 5.0 software.

3. Results and discussion

3.1 CVD on roll-stacked coils

The use of a roll-stacked catalyst coil is a simple and effective method for synthesizing large-area graphene. Ni is an appropriate catalyst for roll-stacked coils because its melting point is much higher than the process temperature. Ni thin films were obtained by thermal evaporation onto one side of the flexible SUS foils and graphene was prepared on the Ni surfaces, as shown in Fig. 1a. The use of Ni thin films enables the control of the number of layers in the graphene film, because less carbon dissolves in thin Ni films than in thick Ni foils.[13,26,27] CVD-grown graphene was grown under the flow of 1.64 vol% CH_4 gas (H_2 : Ar : CH_4 = 100 : 500 : 10 sccm) at 900 °C for

Published on 29 September 2014. Downloaded by Pohang University of Science and Technology on 18/07/2015 09:21:24.

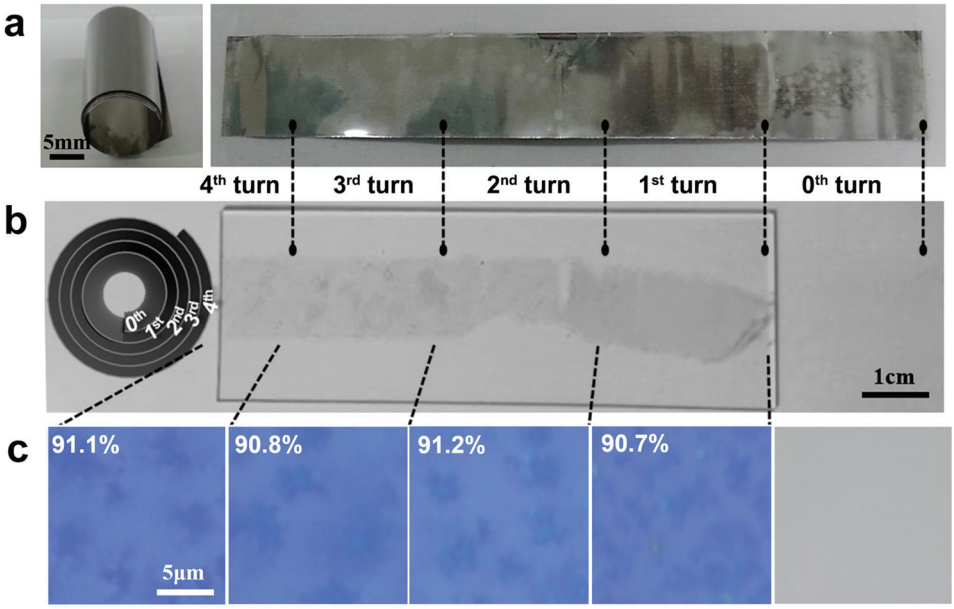

Fig. 1 (a) A roll-stacked Ni coil before and after the CVD process. (b) Schematic diagram of a roll-stacked coil and an image of CVD-grown graphene transferred onto a glass substrate. (c) Optical images of graphene transferred onto a SiO_2/Si wafer from a roll-stacked Ni coil.

10 min, then transferred onto various substrates. As a demonstration, we could obtain a 8 cm × 3 cm (width × length) graphene film in one-pot CVD synthesis using a roll-stacked catalytic coil with an effective dimension of 1 cm × 3 cm (diameter × length), which, beyond doubt, greatly enhanced the productivity of graphene CVD synthesis. Fig. 1c shows optical images of graphene films obtained from the catalytic coil, which was transferred onto 300 nm SiO_2/Si wafers. Interestingly, we found that graphene grew only in the stacked surface region, in which the Ni surfaces faced the bare SUS surfaces (1^{st}–4^{th} turns) but not in the non-stacked surface region where the Ni surface was open to free gas flow (Fig. 1b).

3.2 CVD on multi-stacked substrates

To investigate the growth of graphene on Ni films in a confined geometry, 6 Ni-evaporated flat Si/SiO_2 substrates were stacked in a CVD chamber, as shown schematically in Fig. 2a. The Ni surface on the substrate of the 0^{th} layer was exposed to the free gas flow and the 1^{st}–5^{th} layers were covered by other substrates. Because the Ni film surface is not perfectly flat, we estimated the gap size between the stacked substrates as 135 nm. Since both Si and Fe (SUS) possess higher melting temperatures (1414 °C and 1538 °C, respectively) than the growth temperature (900 °C), the roll-stacked and multi-stacked catalyst systems could be considered analogous except for the interfacial gap size (200 nm for the roll-stacked system) estimated by the physical roughnesses of two facing surfaces (Fig. S4†). The effect of gap sizes will be discussed in detail in section 3.3.1.

As in the roll-stacked system, graphene grew only on the stacked surfaces (the 1^{st}–5^{th} layers) other than exposed, non-stacked surfaces (0^{th} layer) under the flow of 1.64 vol% CH_4 gas. To assess the quality of the synthesized graphene films, the films were transferred to 300 nm thick SiO_2/Si wafers as shown in Fig. 2b. The number of layers in each graphene film was identified from the color contrast in the optical images:[28] the color darkened as the number of graphene layers increased, as shown in this figure. The number of layers was also estimated from the Raman spectroscopy mapping images of the graphene films at 532 nm in Fig. 2c. The spectra contained three main peaks at ~1350 cm^{-1}, ~1585 cm^{-1}, and ~2690 cm^{-1}, which correspond to the D, G, and 2D peaks, respectively. The height ratio of the 2D to the G peaks (I_{2D}/I_G) is related to the graphene sheet thickness; for monolayered graphene, $I_{2D}/I_G > 2$ and for bilayered graphene, $0.7 < I_{2D}/I_G < 1.3$.[29–32] All mappings indicated similar graphene thickness distributions (ESI,† Fig. S1). Monolayers covered 28.6%, 34.7% and 32.9%, and bilayers covered 67.9%, 61.3% and 62.0% of the 1^{st}, 3^{rd}, and 5^{th} Ni substrates, respectively. Moreover, the height ratio of the D to the G peaks (I_D/I_G) is related to the defect density of the graphene sheet. All mappings indicated similar distributions for defect density (ESI,† Fig. S1).[31] Graphene on the stacked Ni films was transferred onto glass substrates. Similar to the properties of the graphene films obtained from the roll-stacked system, the transmittance T of each film from a multi-stacked system was found to be approximately 90% at a wavelength of 550 nm, with a sheet resistance R_s of 4.3 kΩ sq^{-1} averagely, as shown in Fig. 2d. The obtained sheet resistance values were considered reasonable regarding the previous reports on the graphene grown on Ni, which generally show roughly 1–2 kΩ sq^{-1} for 80% transmittance.[13] Therefore, it is reasonable to consider that all the graphene films obtained in this system had similar properties except for the non-stacked catalyst (0^{th} layer). These results indicate that formation of graphene in the confined catalytic geometry underwent different growth behavior, which could

 This journal is © The Royal Society of Chemistry 2015

Published on 29 September 2014. Downloaded by Pohang University of Science and Technology on 18/07/2015 09:21:24.

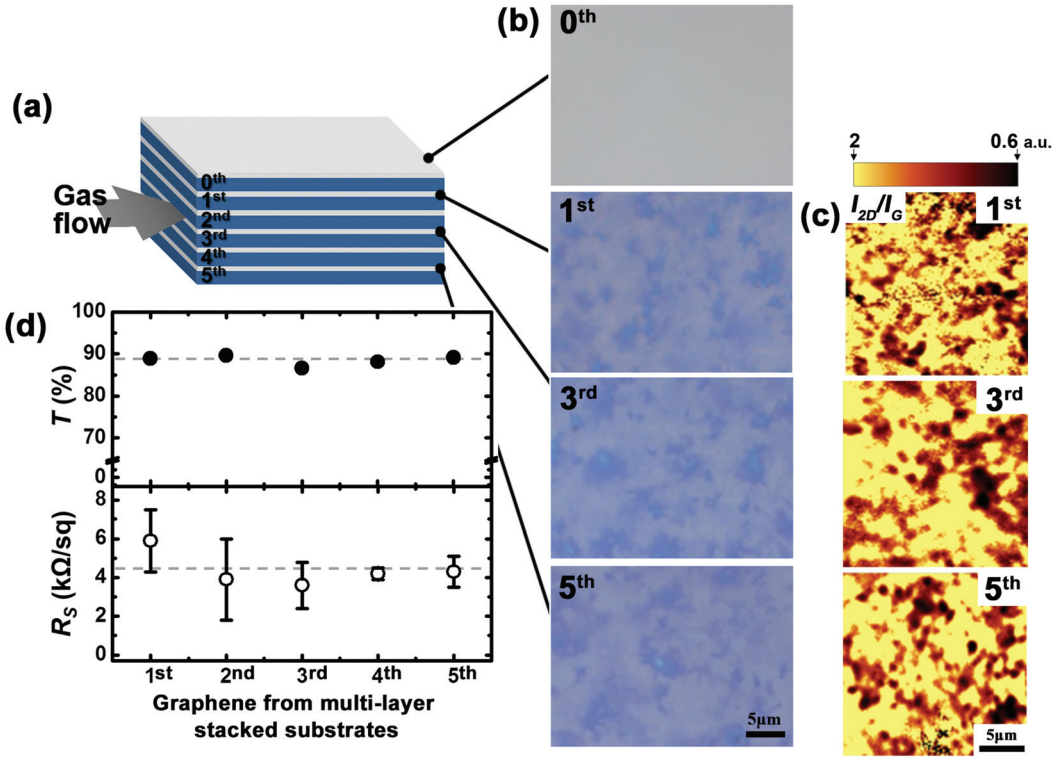

Fig. 2 (a) Schematic diagram of the multi-layer stacked Ni substrates for the CVD-grown graphene. (b) Optical images and (c) Raman 2D-mappings of the graphene films obtained from the multi-layer stacked substrates, 0^{th}, 1^{st}, 3^{rd}, and 5^{th} layers (I_{2D}/I_G, area 400 μm^2). (d) Transmittances and sheet resistances of the graphene films obtained from the multi-layer stacked substrates. Dotted lines indicate the average values of transmittance and sheet resistance.

be ranging from dissolution of carbonaceous species to the segregation and precipitation of dissolved carbon atoms in Ni.

3.3 Graphene growth in a confined geometry

To understand the variation in graphene growth under the confined catalytic geometry, the differences between graphene growth in the stacked system and the non-stacked system were investigated. Graphene growth requires two important steps: (1) dissolution of the carbon source into the Ni surface, and (2) the segregation and precipitation of dissolved carbon atoms on the surface.[33–35] One of the most important factors in the dissolution step is the number of carbon atoms dissolved in the Ni film. In the segregation and precipitation step, the qualities of the Ni surface affect graphene film formation. The dissolution step decides the number of carbon atoms dissolved in the Ni film.

3.3.1. Carbon dissolution in a confined geometry: *Knudsen* molecular flow. In the conventional one-pot CVD process, the Ni surface is completely exposed to the gas flow, as is the case in the non-stacked system. To describe the mass transport of carbon sources to the catalytic surface in graphene growth, previous researchers have used the boundary layer theory of fluid mechanics.[22–25] The main assumption in this theory is the continuum flow where the fluids are regarded as undergoing continuous flow. However, as the gap between the stacks through which the flow passes becomes smaller, the system enters the non-continuum flow regime due to geometric restrictions. In the non-continuum regime, the fluid flow resembles discrete molecular motion because the viscous forces at the walls become dominant. Therefore, the mass transport of the source species for graphene growth is expected to alter significantly when the geometry becomes more confined and the flow regime changes. To characterize this phenomenon, the *Knudsen* flow regime can be used to take into account the effects of the molecular mean-free-path λ and the system dimension d. The ratio, *Knudsen* number, $Kn = \lambda/d$, can be used to distinguish continuum flow from non-continuum flow.[36,37]

Conventionally, $Kn < 0.001$ is the continuum flow regime with non-slip boundary conditions; $0.001 < Kn < 0.1$ is the continuum flow regime with slip boundary conditions; $0.1 < Kn < 10$ is a transition flow regime; $Kn > 10$ is a free molecular flow regime. Transition flow and free molecular flow are within the non-continuum flow regimes, in which each gas molecule collides more often with the wall than with other gas molecules. The gas–gas collision only has a minor effect on the trajectory of gas molecules. Therefore, λ is then limited by the system dimension, which, in our system, can be described as the size of the gap between stacks, L.

Considering the kinetic theory of gases, the collision frequency of gas molecules increases as the λ decreases. However, provided that the total pressure of the system is preserved, two

Published on 29 September 2014. Downloaded by Pohang University of Science and Technology on 18/07/2015 09:21:24.

open-ends of the gap result in decrement of the total number of gas molecules proportional to the decrement of gap size. Therefore, the total gas–wall collision frequency is similar regardless of the gap size. The most significant difference in the *Knudsen* flow regime is the diffusivity, D, of the molecules. Considering that the molecular diffusion is highly dependent on the collision of molecules, the relative diffusivity of the confined system, D_K, with respect to the open, non-stacked system, D_A, is then described by the following equation (see ESI† for details),

$$D_K = \frac{D_A}{Kn}$$

From the above relationship, it can be easily inferred that the prolonged residence of gas molecules within the gap results in higher total collision density, therefore the probability of surface reaction and dissolution of the carbon source into the Ni catalyst can dramatically increase as the *Knudsen* number increases. Once the number of dissolved carbon atoms is sufficient, graphene can form. This postulation is in good agreement with the results for the roll-stacked coil, in which graphene grows on Ni films facing the bare side of the SUS substrate, but not on the open catalytic surface, as already shown in Fig. 1. More systematic investigations of the *Knudsen* flow regime were performed by adjusting the gas flow rates and gap sizes to properly address the importance of considering system dimension on graphene growth under the confined system.

Effects of the carbonaceous gas flow concentration

Firstly, we changed the gas flow rates during the CVD process in both the two-layered stacked system (with a gap size of 135 nm) and the non-stacked system (2 to 50 sccm; CH_4 concentration 0.33 vol% to 7.69 vol% with the flow rates in the proportion H_2 : Ar = 100 : 500 sccm). Graphene films transferred onto the Si substrates consisted of multi-layered graphene sheets, as shown in Fig. 3a , b, as observed for the multi-layered stacked system. In the stacked system, graphene grew even at CH_4 concentrations as low as 0.33 vol% (Fig. 3a), while in the non-stacked system, graphene did not grow at CH_4 concentrations until 10 times higher CH_4 concentration, 3.23 vol% (Fig. 3b). The T and R_s values of the graphene films were measured after they were transferred onto glass substrates. Generally, R_s increases as the number of layers decreases.[38–40] As shown in Fig. 3c, the R_s of graphene obtained from the stacked system was higher than that of non-stacked graphene. At a wavelength of 550 nm, T was 88.5–90.5% for graphene from the two-layered stacked system but only 85.5–87.6% for graphene from the non-stacked system. The average R_s of graphene from the two-layered stacked system was 4.9–6.3 kΩ sq^{-1} (8.3 kΩ sq^{-1} for 0.33 vol% CH_4 flow) and that from the non-stacked system was 1.2–3.2 kΩ sq^{-1}. Interestingly, the values of R_s were remarkably reduced by properly adjusting the gap size in the stacked system (down to 1.6 kΩ sq^{-1}), while preserving the high transparency (T > 89%) (Fig. 3c). These results indicate that other than the low-onset of graphene growth with respect to CH_4 concentration, the confined geometry could also elevate the quality and homogeneity of the synthesized graphene films (discussed in detail in the section 3.3.2).

Raman spectra were taken from five locations of each graphene films grown under each condition (ESI,† Fig. S2). The spectrum showed three main peaks at ~1350 cm^{-1}, ~1585 cm^{-1}, and ~2690 cm^{-1}, corresponding to D, G, and 2D peaks, respectively. The ratio of the 2D to G peaks (I_{2D}/I_G) indicated that single-, bi-, and multi-layered graphene sheets formed in various areas, and that the stacked system produced more mono- and bilayered sheets than the non-stacked system (ESI,† Fig. S3).

Aside from the quality variation (will be explained in the later section), firstly, we investigated the criteria for the onset of graphene growth with respect to the CH_4 concentration. The *Knudsen* number of our stacked, confined system was estimated by calculating the mean free path as follows,

$$\lambda = \frac{k_B K}{\sqrt{2}\pi\sigma^2 p}$$

where k_B = Boltzmann constant [1.38×10^{-23} (kg m^2 s^{-2}) K^{-1}], K = thermodynamic temperature [900 °C = 1173.15 K], σ = particle hard shell diameter [diameter of the CH_4 molecule = 0.38 nm], and p = total pressure [1.6 Torr = 213.3 kg (m s^{-2})$^{-1}$].

We calculated that $\lambda \approx 119$ μm and estimated that $L \approx 135$ nm because the upper substrate and the Ni film substrate are not perfectly flat: the maximum height of the Ni film surface was 69.7 nm after CVD and the height of the back side of the upper substrate was approximately 65 nm (ESI,† Fig. S4). In this system Kn = 881.5, which was well over 10, therefore, the gas flow through the gap is in the free molecular flow regime. Furthermore, we estimated $L \approx 200$ nm in the roll-stacked system (Kn = 595), because the maximum height of the SUS surface was 130 nm (ESI,† Fig. S4). In the case of hydrogen, which is already known to have a minor effect on the dissolution step of graphene CVD growth on Ni,[41] it is expected to have relatively similar kinetic behavior to the non-stacked system due to much smaller molecular radius (0.12 nm) and consequently a shorter λ than methane. Therefore, together with the fact that only gas-wall collision prevailed in the *Knudsen* flow regime, it is reasonable to consider that the stacked system majorly affected the CH_4 gas flow which directly decided the resulting dissolution step.

In the stacked system, as indicated by large Kn, the diffusivity of CH_4 gas molecules within the gap channel was significantly enhanced, so that the increased dissolution of carbon species into Ni results in at least, considering instrumental allowance, 10 times lower CH_4 concentration for the onset of graphene growth (3.23 vol% to 0.33 vol%). It has been reported that the segregation limit (single and few layered graphene growth) of carbon concentration (c_s) in Ni is about 5.1×10^{20} carbon atoms cm^{-3} at 900 °C.[34] Therefore, in the non-stacked system, we can safely speculate that the spontaneously dissolved carbon concentration in Ni film at 3.23 vol% CH_4 flow was near c_s. Since we used a 400 nm thick Ni film at 3.23 vol% CH_4 flow, the dissolved carbon concentration per area of Ni

 This journal is © The Royal Society of Chemistry 2015

Published on 29 September 2014. Downloaded by Pohang University of Science and Technology on 18/07/2015 09:21:24.

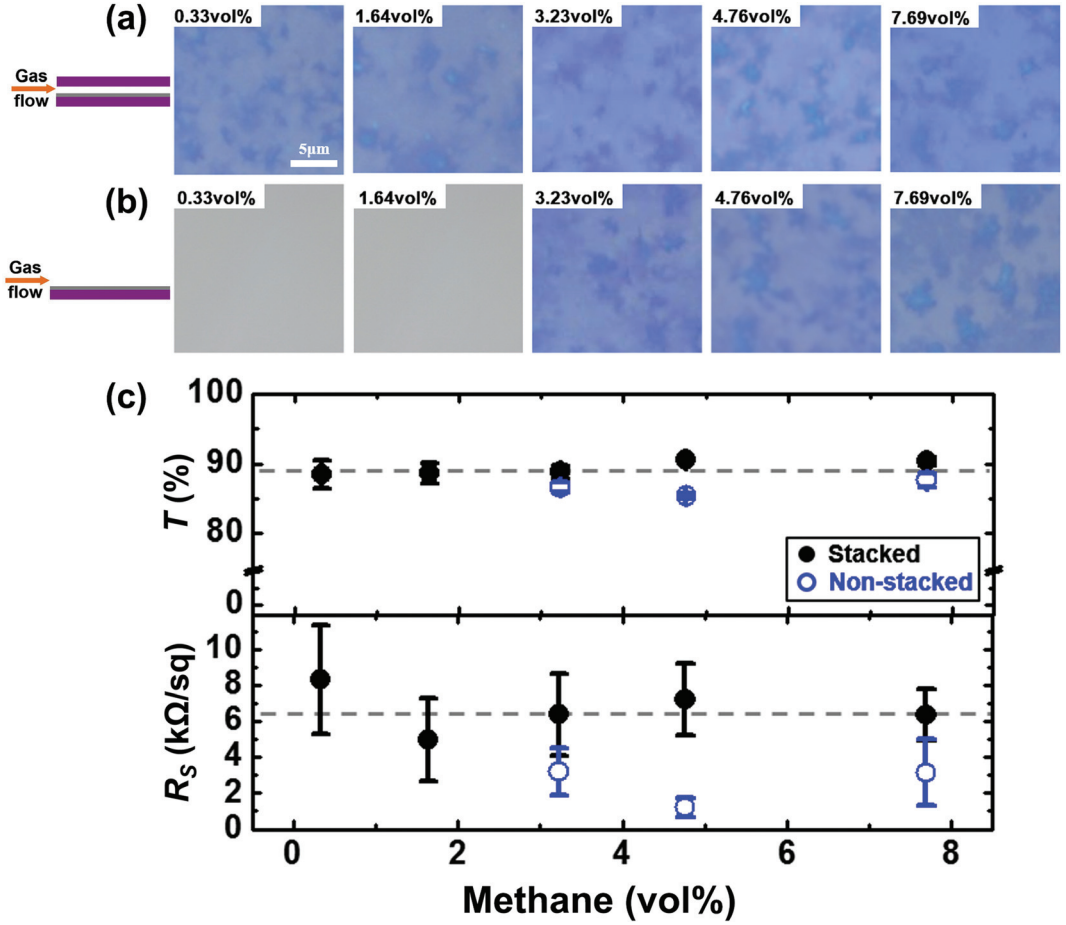

Fig. 3 Optical images of graphene films transferred onto SiO_2/Si wafers (a) grown in the bi-layer stacked system under various CH_4 concentrations, 0.33–7.69 vol%, and (b) grown in the non-stacked system under various CH_4 concentrations, 0.33–7.69 vol%. (c) Transmittances and sheet resistances of graphene obtained at each CH_4 concentration. Dotted lines indicate the average values of transmittance and sheet resistance.

was about 1.9×10^{16} carbon atoms cm^{-2}, which, considering atomic density of graphene (3.8×10^{15} carbon atoms cm^{-2}), corresponded to the areal density of approximately 5 homogeneous graphene layers.

In kinetic theory of gases, gas-wall collision frequency is directly proportional to the gas concentration. Therefore, 1/10 of gas flow, *i.e.* 0.33 vol% of CH_4 flow, only guaranteed 0.51 of graphene layer in the non-stacked system, which was not sufficient to form even a single graphene layer. Surprisingly, in the case of the stacked system, 0.33 vol% of CH_4 successfully induced the formation of an average of 1.98 layers of fully covered graphene over the entire catalytic surface, therefore indicating at least 10 times higher dissolution probability than the non-covered system. Furthermore, regarding the abundance of carbon source flow (5.4×10^{20} molecules per 10 min, 2 sccm), it can also be expected that precipitation (amorphous carbon growth) rather than segregation could have occurred in the stacked system at a given large *Knudsen* number.[34,41] However, until 7.69 vol% (50 sccm) of CH_4 flow, no precipitation occurred for both the stacked and non-stacked systems. The limited number of CH_4 molecules due to small gap, assuming homogeneous gas flux for both inside and outside the gap, would have suppressed the overdose of dissolved carbon in Ni. From the above results, it can be reasonably concluded that the increased carbon dissolution probability of the stacked system only gives rise to sufficient carbon concentration for the growth of graphene, rather than for precipitation of amorphous carbon. Moreover, considering inhomogeneous dissolved-carbon distribution across the Ni grain boundaries, the graphene growth would have been spurred by the possible change in the morphology of Ni surfaces. However, the increased portion of the (111) crystalline plane, enlarged grain size, and decreased surface roughness (Fig. 5) in the stacked system indicate that low CH_4 concentration for the onset of graphene growth could not be promoted by surface characteristics of Ni. These changes rather enhanced the quality (distribution of number of layers) of synthesized graphene. This will be discussed in detail in section 3.3.2.

Effects of the gap size variation

So far, we have successfully assessed the variation in dissolution probability by introducing the *Knudsen* flow regime. As a next step, we systematically varied the *Knudsen* number and investigated its effect on graphene growth by directly varying

Published on 29 September 2014. Downloaded by Pohang University of Science and Technology on 18/07/2015 09:21:24.

gap sizes in the range 135 nm < L < 1.2 mm; λ = 119 μm was fixed for the CH_4 flow. A gas mixture containing 1.64 vol% of CH_4 concentration was passed through the gap, and the CVD chamber was heated to 900 °C. When L = 10 μm, Kn = 11.9, so the gas flow was in the free molecular flow regime; when L > 1.2 mm, Kn < 0.01, so the flow was in the slip flow regime; when 10 μm < L < 1.2 mm, the flow was in the transition flow regime (ESI,† Table S1). From the results in the previous section, it was safe to expect that 5 times larger gap size than minimum gap (135 nm, Kn = 881.5) would be sufficient to spur the growth of graphene at this CH_4 concentration. In theory, Kn of at least 2 was required to provide dissolved carbon concentration above the segregation limit in the stacked system at 1.64 vol% CH_4 flow. However, as the Kn decreased under 10–0.1, as in the transition regime, the diffusion of gas molecules was no longer solely limited by gas-wall collision, but was also affected by the presence of other gas molecules. The cumulative contribution of both collisions decides the overall diffusivity of gas molecules. Therefore, in the transition regime, it can be deduced that the diffusivity becomes lower than expected from extension of free-molecular flow.

In our system, graphene films were formed for L < 600 μm (Kn > 0.2) (Fig. 4a) of which the T at 550 nm was ~90%, and R_s was 1.8–4.8 kΩ sq^{-1} (Fig. 4b). Graphene grew in both the free molecular flow regime (135 nm < L < 10 μm) and the transition flow regime (30 μm < L < 600 μm), but not in the slip flow regime (L = 1.2 mm), as shown in Fig. 4a, b. Therefore, the relative criterion for graphene growth at 10 sccm (1.64 vol%) of CH_4 flow was Kn > 0.1, just within the boundary of the transition flow regime. Considering similar estimated dimensions of geometric confinement in the roll-stacked (200 nm) and the simple stacked (135 nm) systems, the *Knudsen* number of the roll-stacked system also satisfactorily met the criteria for the graphene growth, which agreed well with the observed graphene growth behaviors in sections 3.3.1 and 3.3.2.

Although these analyses based on *Knudsen* molecular flow explained the overall trends in graphene growth, the quality of graphene could not be estimated by only the *Knudsen* flow theory. It is well known that the quality of graphene is mainly decided by the segregation and precipitation step rather than the dissolution step, provided that dissolved carbon concentration is well within the window of the segregation limit.[34] As

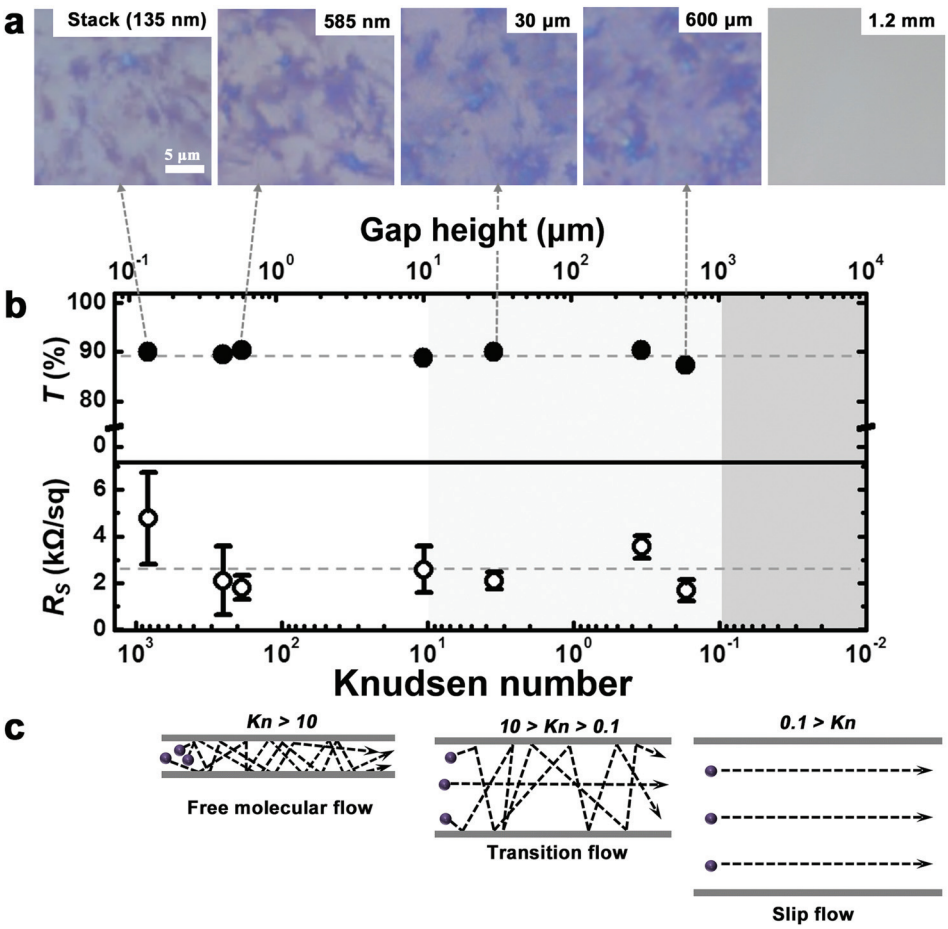

Fig. 4 (a) Optical images of graphene films transferred onto SiO_2/Si wafers after synthesis with gaps in the range 135 nm–1.2 mm. (b) Transmittances and sheet resistances of CVD-grown graphene. Dotted lines indicate the average values of transmittance and sheet resistance. (c) Schematic diagram of the flow regimes.

 This journal is © The Royal Society of Chemistry 2015

Published on 29 September 2014. Downloaded by Pohang University of Science and Technology on 18/07/2015 09:21:24.

mentioned earlier, the limited amount of maximum dissolved carbon in 400 nm Ni was well within the segregation limit, so that the difference in graphene quality (Fig. 5, Fig. S3†) mainly originated from the variation in the segregation and precipitation step.

3.3.2 Segregation and precipitation step. In the segregation and precipitation step, the rate of temperature cooling and the metal surface properties have critical influences, because they determine the number of layers in CVD-grown graphene.[42–48] To reduce the amount of multi-layered gra-

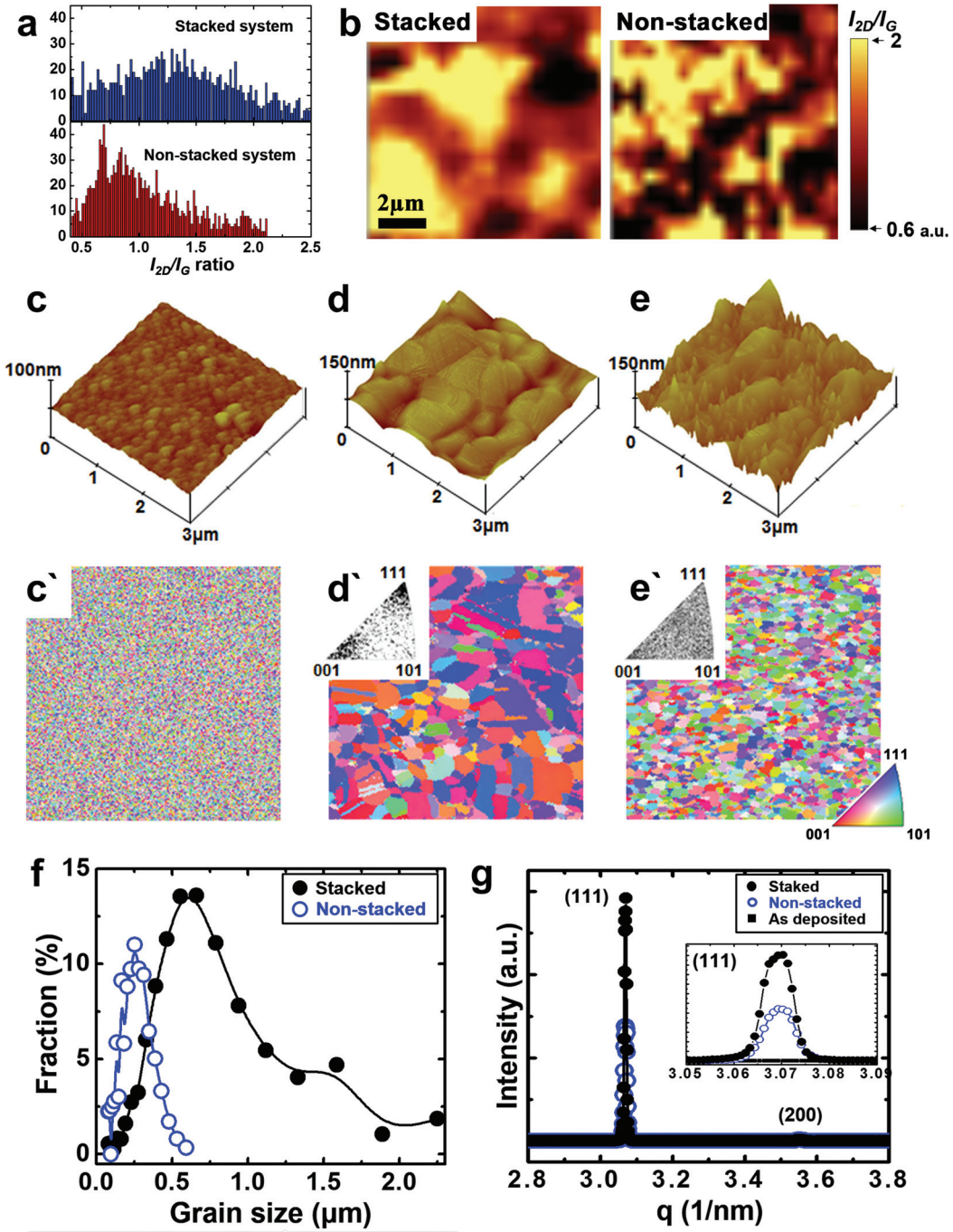

Fig. 5 (a) Statistical distribution and (b) 2D-mapping image of the Raman I_{2D}/I_G ratio of graphene films synthesized in the bi-layer stacked and non-stacked systems under 4.76 vol% of CH_4 concentration (area 100 μm^2). AFM images of (c) an as-evaporated Ni surface and Ni surfaces heat-treated under a H_2/Ar atmosphere in (d) stacked and (e) non-stacked systems. (f) Grain size distributions for heat-treated Ni films obtained with EBSD. Normal-directional EBSD mapping of (c′) the as-evaporated Ni surface and the Ni surfaces thermally treated under a H_2/Ar atmosphere of the (d′) stacked and (e′) non-stacked systems. The colors represent the orientations of the polycrystalline Ni films after heat treatment. (g) XRD spectra; the inset shows the (111) peak.

Published on 29 September 2014. Downloaded by Pohang University of Science and Technology on 18/07/2015 09:21:24.

phene, the number of grain boundaries in the polycrystalline Ni films should be decreased, because the dissolved carbon atoms in the Ni films easily come out through the grain boundaries and form the multi-layered graphene.[44,45] In addition, the proportion of the (111) plane should be increased in the polycrystalline Ni films.[46–48] In the stacked system, the stack might induce change in the crystallographic or/and morphological properties of the Ni catalyst, which could exert large influence on segregated graphene quality. Moreover, as briefly mentioned in section 3.3.1, it is worth pointing out that the change of surface characteristics can also affect the segregation limit of carbon concentration, considering the possible increment in the inhomogeneity of carbon distribution across the grain boundaries. In this sense, we carefully examined the morphological and crystallographic characteristics of the Ni surfaces.

Morphology of Ni surfaces

Fig. 5a and b show the quality of graphene under the stacked system. It is clear that distribution of I_{2D}/I_G in the stacked system had larger domains and was more dedicated to higher values, which indicated homogeneous and monolayer growth of graphene. As mentioned before, the graphene quality, *i.e.* homogeneity and relative portion of monolayered graphene, is mainly decided by the segregation and precipitation step, which is influenced by surface morphology and crystallographic orientation of Ni surfaces. Atomic force microscopy (AFM) was used to examine the Ni film surface to determine how the quality of the Ni film after annealing under low-pressure H_2/Ar affects graphene synthesis. AFM images of an evaporated Ni film were obtained prior to heat treatment (Fig. 5c), and after annealing the Ni surfaces in the stacked system (Fig. 5d) and in the non-stacked system (Fig. 5e). After annealing at 900 °C, the surface roughness (RMS) of the stacked system was 8.7 nm and that of the non-stacked system was 23.8 nm. The maximum height of the Ni films in the stacked system was 69.7 nm and that of the non-stacked system was 270.9 nm. In the images, it can be seen that the grains were larger and smoother in the stacked system than in the non-stacked system; *i.e.*, the Ni surfaces of the stacked system were flatter and had fewer grain boundaries than the non-stacked system; stacking the substrates resulted in the flattening of the Ni crystals due to the external strain physical confinement, which reduced the evaporative loss of metal.[49,50] Decreasing the number of grain boundaries and smoothing the Ni surface might reduce the amount of multi-layered graphene, which increased the transmittance T of graphene. As the gap size increased, the surfaces became gradually rough, but still showed smooth domains without any development of small spike-like features as in non-stacked systems (ESI,† Fig. S5). After annealing, the Ni surface for a gap size of 30 μm has RMS = 17.4 nm and maximum height = 137.2 nm, and for a gap size of 1.2 mm RMS = 24.1 nm and the maximum height = 170.3 nm. These results agreed well with the measured average sheet resistance R_s of graphene films obtained by adjusting the gap size, which was around 2.3 kΩ sq^{-1} at T of 89.4%, as shown in Fig. 4b. With smoother grains, the synthesized graphene films were not only transparent but also highly conductive. Increasing the gap size slightly increased the R_s up to 3 kΩ sq^{-1}, but still preserved high T above 90%, indicating higher homogeneity of graphene films synthesized under the stacked system than the non-stacked system. For the closely stacked system (135 nm gap), the slightly higher measured R_s (4.9 kΩ sq^{-1}) could be a result of the physical interruption of graphene growth on the Ni surface contacted with the upper substrate, and possibly from the increased etching of carbon species by significantly reducing the H_2 diffusion rate at the smallest gap. Electron backscattered diffraction (EBSD) also indicated that the stacked system had larger grains with a larger range of sizes than the non-stacked system, as could be seen in Fig. 5f. Thus, the stacked system had fewer grain boundaries than the non-stacked system.

Clearly, the introduction of the confined catalytic geometry promoted reduction in the surface roughness and decrement in the number of grain boundaries of the Ni catalyst as the gap narrowed. These variations in the Ni surface resulted in enhancement of graphene quality by reducing graphene nucleation sites such as grain boundaries and defects. Moreover, since this reduction generally increased the segregation limit on carbon concentration, the growth of graphene even at low CH_4 concentration (0.33 vol%) in the stacked system conclusively eliminated the possibility that the change of Ni morphology promoted the onset of graphene growth at low CH_4 concentration in the stacked system, as suggested earlier in section 3.3.1.

Crystallographic characteristics of Ni

The annealed Ni surfaces were examined to determine how their crystallographic characteristics affect the synthesized graphene films. Increases in the (111) peak intensity and in the (111) grain size of the Ni films increase the probability that graphene will form either monolayers or bilayers.[46,47] Crystalline orientation maps for the normal direction of the Ni films were obtained with EBSD. Three grain orientations, (111), (001), and (101) were evident in Fig. 5c′–e′. The EBSD mapping of the as-evaporated Ni film surface prior to heat treatment indicated that there were no specific crystalline domains, as shown in Fig. 5c′. However, specific crystalline domains developed after heat treatment. The crystalline domains were larger in the stacked system (Fig. 5d′) than in the non-stacked system (Fig. 5e′). As the crystalline domains developed, the (111) directions developed effectively in the stacked system, but no preferred orientation was evident in the non-stacked system. The out-of-plane X-ray diffraction patterns of the three Ni films also showed that there was no preferred intensity of reflections in the as-evaporated Ni film, but there were large increases in the intensities of the (111) reflections at q = 3.07 nm^{-1} after thermal annealing, as shown in Fig. 5g. However, during the annealing process, the crystallinity of the (111) plane of the Ni surface in the stacked system increased; the intensity of the (111) peak was twice as high in the stacked system as in the non-stacked system. As a result, the crystal orientation of the

 This journal is © The Royal Society of Chemistry 2015

Published on 29 September 2014. Downloaded by Pohang University of Science and Technology on 18/07/2015 09:21:24.

stacked Ni surface increased in the proportions of mono- and bilayered graphene (Fig. 5a, b and Fig. S3†). These observations also agreed well with the previous results, as in Ni morphology and graphene quality.

3.4 Application of roll-synthesized graphene

The development of flexible transparent conducting films (TCFs) is a key to the realization of flexible electronics. The graphene-based TCFs have intrinsic flexibility and transparency along with high electrical properties, which make graphene TCF a highly feasible flexible TCF for real application.[51] In this sense, a low-energy consuming, high-throughput production of graphene sheets is a basic step toward soft electronics. To demonstrate the applicability of our method, we fabricated graphene based flexible TCFs and flexible organic field effect transistor (OFET) arrays on plastic. We could obtain 8 cm × 3 cm (width × length) flexible graphene TCFs on the PET film *via* the one-pot CVD synthesis based on the roll-stacked catalytic coil with an effective dimension of 1 cm × 3 cm (diameter × length), which increased the productivity of graphene synthesis by almost one order. We also demonstrated a pentacene based organic transistor on plastic using pattern-transferred graphene as source/drain electrodes. The device showed stable operation with a hole mobility of 0.51 $cm^2\ V^{-1}\ s^{-1}$ and high mechanical stability (ESI,† Fig. S6).

4. Conclusions

We have demonstrated a high-throughput CVD synthesis of graphene on polycrystalline Ni films using a roll-stacked catalytic coil, and systematically studied the graphene growth mechanism on confined catalytic substrates. Graphene was successfully synthesized at very low CH_4 concentrations in a confined geometry, of which the gas flow was characterized as the free molecular flow and transition flow regimes ($Kn > 0.1$). Moreover, the confined geometry also altered the evolution of the morphological and crystallographical structure of the Ni films during the CVD process. Reducing the gap size increased the size of the Ni grains and promoted the predominant development of (111) crystal orientation on the surface of the Ni catalyst. As a consequence, the proportion of mono- and bilayered components of the graphene film was increased and the number of graphene layers showed narrow distribution, which resulted in the increased homogeneity of the synthesized graphene sheets.

This work provides a simple and efficient method to maximize the catalytic area without unnecessary time and energy consumption. Moreover, we believe that the controlled evolution of the catalytic surface in our work might provide a new avenue for high quality and large-area graphene synthesis, which possesses high feasibility for a wide range of applications such as soft electronics based on both organic semiconductors and graphene electrodes.

Acknowledgements

This work was supported by a grant (code no. 2011-0031628) from the Center for Advanced Soft Electronics under the Global Frontier Research Program of the Ministry of Science, ICT & Future Planning, Korea. The authors thank the Pohang Accelerator Laboratory for providing the synchrotron radiation sources at 9C, 1D and 3D beam lines used in this study.

Notes and references

1 C. Lee, X. D. Wei, J. W. Kysar and J. Hone, *Science*, 2008, **321**, 385–388.
2 A. A. Balandin, *Nat. Mater.*, 2011, **10**, 569–581.
3 T. G. Pedersen, C. Flindt, J. Pedersen, A. P. Jauho, N. A. Mortensen and K. Pedersen, *Phys Rev B: Condens. Matter*, 2008, **77**, 245431.
4 W. H. Lee, J. Park, Y. Kim, K. S. Kim, B. H. Hong and K. Cho, *Adv. Mater.*, 2011, **23**, 3460–3464.
5 Y. W. Tan, Y. Zhang, K. Bolotin, Y. Zhao, S. Adam, E. H. Hwang, S. Das Sarma, H. L. Stormer and P. Kim, *Phys. Rev. Lett.*, 2007, **99**, 246803.
6 S. Adam, E. H. Hwang, V. M. Galitski and S. Das Sarma, *Proc. Natl. Acad. Sci. U. S. A.*, 2007, **104**, 18392–18397.
7 H. H. Kim, J. W. Yang, S. B. Jo, B. Kang, S. K. Lee, H. Bong, G. Lee, K. S. Kim and K. Cho, *Acs Nano*, 2013, **7**, 1155–1162.
8 K. S. Novoselov, A. K. Geim, S. V. Morozov, D. Jiang, Y. Zhang, S. V. Dubonos, I. V. Grigorieva and A. A. Firsov, *Science*, 2004, **306**, 666–669.
9 K. V. Emtsev, A. Bostwick, K. Horn, J. Jobst, G. L. Kellogg, L. Ley, J. L. McChesney, T. Ohta, S. A. Reshanov, J. Rohrl, E. Rotenberg, A. K. Schmid, D. Waldmann, H. B. Weber and T. Seyller, *Nat. Mater.*, 2009, **8**, 203–207.
10 W. A. d. Heer and C. Berger, *J. Phys. D: Appl. Phys.*, 2012, **45**, 150301.
11 C. Riedl, C. Coletti and U. Starke, *J. Phys. D: Appl. Phys.*, 2010, **43**, 374009.
12 J. Hwang, M. Kim, D. Campbell, H. A. Alsalman, J. Y. Kwak, S. Shivaraman, A. R. Woll, A. K. Singh, R. G. Hennig, S. Gorantla, M. H. Rummeli and M. G. Spencer, *Acs Nano*, 2013, **7**, 385–395.
13 K. S. Kim, Y. Zhao, H. Jang, S. Y. Lee, J. M. Kim, K. S. Kim, J.-H. Ahn, P. Kim, J.-Y. Choi and B. H. Hong, *Nature*, 2009, **457**, 706–710.
14 G. Faggio, A. Capasso, G. Messina, S. Santangeo, T. Dikonimos, S. Gagliardi, R. Giorgi, V. Morandi, L. Ortolani and N. Lisi, *J. Phys. Chem. C*, 2013, **117**, 21569–21576.
15 H. Kim, I. Song, C. Park, M. Son, M. Hong, Y. Kim, J. S. Kim, H.-J. Shin, J. Baik and H. C. Choi, *Acs Nano*, 2013, **7**, 6575–6582.
16 S. Bae, H. Kim, Y. Lee, X. Xu, J. S. Park, Y. Zheng, J. Balakrishnan, T. Lei, H. Ri Kim, Y. I. Song, Y. J. Kim, K. S. Kim, B. Özyilmaz, J. H. Ahn, B. H. Hong and S. Iijima, *Nat. Nanotechnol.*, 2010, **5**, 574–578.

Published on 29 September 2014. Downloaded by Pohang University of Science and Technology on 18/07/2015 09:21:24.

17 C. D. Liao, Y. Y. Lu, S. R. Tamalampudi, H. C. Cheng and Y. T. Chen, *J. Phys. Chem. A*, 2013, **117**, 9454–9461.
18 L. David, R. Bhandavat, G. Kulkarni, S. Pahwa, Z. Zhong and G. Singh, *ACS Appl. Mater. Inter.*, 2013, **5**, 546–552.
19 T. Kobayashi, M. Bando, N. Kimura, K. Shimizu, K. Kadono, N. Umezu, K. Miyahara, S. Hayazaki, S. Nagai, Y. Mizuguchi, Y. Murakami and D. Hobara, *Appl. Phys. Lett.*, 2013, **102**, 023112.
20 Y. Zhang, L. Zhang, P. Kim, M. Ge, Z. Li and C. Zhou, *Nano Lett.*, 2012, **12**, 2810–2816.
21 M. H. Rümmeli, S. Gorantla, A. Bachmatiuk, J. Phieler, N. Geißler, I. Ibrahim, J. Pang and J. Eckert, *Chem. Mater.*, 2013, **24**, 4861–4866.
22 C. Jia, J. Jiang, L. Gan and X. Guo, *Sci. Rep.*, 2012, **2**, 1–6.
23 S. Bhaviripudi, X. T. Jia, M. S. Dresselhaus and J. Kong, *Nano Lett.*, 2010, **10**, 4128–4133.
24 A. M. Lewis, B. Derby and I. A. Kinloch, *Acs Nano*, 2013, **7**, 3104–3117.
25 S.-Y. Cho, K.-J. Kim, H.-M. Kim, D.-J. Lee, M.-H. Lee and K.-B. Kim, *RSC Adv.*, 2013, **3**, 26376–26381.
26 M. G. Rybin, A. S. Pozharov and E. D. Obraztsova, *Phys. Status Solidi C*, 2010, **7**, 2785–2788.
27 J. J. Lander, H. E. Kern and A. L. Beach, *J. Appl. Phys.*, 1952, **23**, 1305–1309.
28 C. M. Nolen, G. Denina, D. Teweldebrhan, B. Bhanu and A. A. Balandin, *Acs Nano*, 2011, **5**, 914–922.
29 K. Yan, H. L. Peng, Y. Zhou, H. Li and Z. F. Liu, *Nano Lett.*, 2011, **11**, 1106–1110.
30 Z. Yan, Z. W. Peng, Z. Z. Sun, J. Yao, Y. Zhu, Z. Liu, P. M. Ajayan and J. M. Tour, *Acs Nano*, 2011, **5**, 8187–8192.
31 A. C. Ferrari, J. C. Meyer, V. Scardaci, C. Casiraghi, M. Lazzeri, F. Mauri, S. Piscanec, D. Jiang, K. S. Novoselov, S. Roth and A. K. Geim, *Phys. Rev. Lett.*, 2006, **97**, 187401.
32 J. Lee, K. S. Novoselov and H. S. Shin, *Acs Nano*, 2011, **5**, 608–612.
33 X. S. Li, W. W. Cai, L. Colombo and R. S. Ruoff, *Nano Lett.*, 2009, **9**, 4268–4272.
34 L. Baraton, Z. B. He, C. S. Lee, C. S. Cojocaru, M. Chatelet, J. L. Maurice, Y. H. Lee and D. Pribat, *EPL*, 2011, **96**, 46003.
35 R. S. Weatherup, B. C. Bayer, R. Blume, C. Baehtz, P. R. Kidambi, M. Fouquet, C. T. Wirth, R. Schlogl and S. Hofmann, *Chemphyschem*, 2012, **13**, 2544–2549.
36 K. Xu and Z. H. Li, *J. Fluid Mech.*, 2004, **513**, 87–110.
37 D. A. Nield and A. V. Kuznetsov, *Transp. Porous Med.*, 2006, **64**, 161–170.
38 D. Y. Wan, T. Q. Lin, H. Bi, F. Q. Huang, X. M. Xie, I. W. Chen and M. H. Jiang, *Adv. Funct. Mater.*, 2012, **22**, 1033–1039.
39 S. S. Chen, W. W. Cai, R. D. Piner, J. W. Suk, Y. P. Wu, Y. J. Ren, J. Y. Kang and R. S. Ruoff, *Nano Lett.*, 2011, **11**, 3519–3525.
40 G. Jo, M. Choe, S. Lee, W. Park, Y. H. Kahng and T. Lee, *Nanotechnology*, 2012, **23**, 112001.
41 M. Losurdo, M. M. Giangregorio, P. Capezzuto and G. Bruno, *Phys. Chem. Chem. Phys.*, 2011, **13**, 20836–20843.
42 K. Xiao, H. Wu, H. Lv, X. Wu and H. Qian, *Nanoscale*, 2013, **5**, 5524–5529.
43 Q. Yu, J. Lian, S. Siriponglert, H. Li, Y. P. Chen and S.-S. Pei, *Appl. Phys. Lett.*, 2008, **93**, 113103.
44 Y. Zhang, L. Gomez, F. N. Ishikawa, A. Madaria, K. Ryu, C. A. Wang, A. Badmaev and C. W. Zhou, *J. Phys. Chem. Lett.*, 2010, **1**, 3101–3107.
45 Y. Xue, B. Wu, Y. Guo, L. Huang, L. Jiang, J. Chen, D. Geng, Y. Liu, W. Hu and G. Yu, *Nano Res.*, 2011, **4**, 1208–1214.
46 J. Wintterlin and M. L. Bocquet, *Surf. Sci. Spectra*, 2009, **603**, 1841–1852.
47 S. Thiele, A. Reina, P. Healey, J. Kedzierski, P. Wyatt, P. L. Hsu, C. Keast, J. Schaefer and J. Kong, *Nanotechnology*, 2010, **21**, 015601.
48 S. J. Kim, D. W. Kim and H. T. Jung, *RSC Adv.*, 2013, **3**, 22909–22913.
49 C. A. Volkert and C. Lingk, *Appl. Phys. Lett.*, 1998, **73**, 3677–3679.
50 A. M. Deus, M. A. Fortes, P. J. Ferreira and J. B. V. Sande, *Acta Mater.*, 2002, **50**, 3317–3330.
51 S. B. Jo, J. Park, W. H. Lee, K. Cho and B. H. Hong, *Solid State Commun.*, 2012, **152**, 1350–1358.

 This journal is © The Royal Society of Chemistry 2015